VARIATIONAL MULTISCALE METHODS FOR LARGE EDDY SIMULATION OF TURBULENT FLOWS: FOURIER ANALYSIS AND APPLICATION TO DIFFUSER FLOW

Volker Gravemeier
Emmy Noether Research Group,
Chair for Computational Mechanics,
Technical University of Munich
Boltzmannstr. 15, D-85748 Garching, Germany
vgravem@lnm.mw.tum.de

Martin Kronbichler
Division of Scientific Computing,
Department of Information Technology,
Uppsala University
Box 337, SE-751 05 Uppsala, Sweden
martin.kronbichler@it.uu.se

Wolfgang A. Wall
Chair for Computational Mechanics,
Technical University of Munich
Boltzmannstr. 15, D-85748 Garching, Germany
wall@lnm.mw.tum.de

ABSTRACT

A variational multiscale large eddy simulation (VMLES) based on an h-type scale separation is derived. Within this method, a standard Smagorinsky model is applied to the smaller of the resolved scales in order to account for the effect of unresolved scales. The larger resolved scales do not contain any modeling term. To separate large and small resolved scales, two grids of different characteristic length are introduced – a fine grid for the resolved scales and a coarser grid for the identification of the large resolved scales. The application of the method to turbulent flow in a diffuser shows the good features of the VMLES already for relatively coarse resolutions. Additionally, a tool based on Fourier analysis is derived, enabling a straightforward classification of scale-separating procedures based on a one-dimensional test equation.

INTRODUCTION

In many engineering problems, one faces the need to examine the motion of fluids. A mathematical formulation of the fluid motion is provided by the Navier-Stokes equations. Since no analytical solution is known for most flows, numerical simulation is an essential tool for the study and prediction of real flow situations, particularly for turbulent flows. The coupling of all scales in the flow makes it necessary to examine the whole range of active scales. Though, the more turbulence is in the flow, the larger gets this range. Hence, a direct numerical simulation (DNS) resolving all scales is usually not a viable approach. One alternative to overcome this problem is large eddy simulation (LES), where only larger scales are resolved, whereas the effect of the unresolved small scales on the resolved larger scales is modeled. Traditional LES approaches do not yet perform satisfactorily for certain applications. A very promising approach towards an improved LES is the variational multiscale large eddy simulation (VMLES), see, e.g., Hughes *et al.* (2000) and Gravemeier (2006b). In the VMLES, only the effect of the unresolved scales on the smaller of the resolved scales is modeled, whereas no modeling term is added to the larger of the resolved scales. In this paper, a VMLES suitable for use within both a finite element and a finite volume method is presented in a finite element setting, with the separation between large and small resolved scales realized by an h-type approach. Afterwards, an application of such an h-type scale separation within a finite volume method to turbulent flow in a planar asymmetric diffuser is described. Furthermore, a Fourier analysis in a simple 1D setting is carried out.

NAVIER-STOKES EQUATIONS AND VMLES

Incompressible Navier-Stokes Equations

The objective is to solve the Navier-Stokes equations for incompressible flow in a bounded, connected domain Ω: Find a velocity field $\mathbf{u}$ and a pressure field p such that

$$\frac{\partial \mathbf{u}}{\partial t} + \nabla \cdot (\mathbf{u} \otimes \mathbf{u}) - 2\nu \nabla \cdot \varepsilon(\mathbf{u}) + \nabla p = \mathbf{f} \tag{1}$$

$$\nabla \cdot \mathbf{u} = 0 \tag{2}$$

for $0 < t \leq T$ and all $\mathbf{x} \in \Omega$. At $t = 0$, it is required that $\mathbf{u}(\cdot, 0) = \mathbf{u}_0$ for a prescribed divergence-free initial velocity field $\mathbf{u}_0$. In (1)-(2), $\mathbf{f}$ is a given body force and ν the kinematic viscosity of the fluid. $\varepsilon(\mathbf{u}) = 1/2(\nabla \mathbf{u} + (\nabla \mathbf{u})^T)$ denotes the rate-of-deformation tensor.
At the boundary $\Gamma \times (0, T] = \partial\Omega \times (0, T]$, Dirichlet and

Neumann boundary conditions are applied, respectively,

$$\mathbf{g} = \mathbf{u} \quad \text{on} \quad \Gamma_{\mathrm{D}} \times (0, T] \tag{3}$$

$$\mathbf{h} = p\mathbf{n} + 2\nu\varepsilon(\mathbf{u}) \cdot \mathbf{n} \quad \text{on} \quad \Gamma_{\mathrm{N}} \times (0, T] \tag{4}$$

for $\Gamma_{\mathrm{D}} \cap \Gamma_{\mathrm{N}} = \emptyset$ and $\Gamma_{\mathrm{D}} \cup \Gamma_{\mathrm{N}} = \Gamma$, with $\mathbf{n}$ denoting the outer normal to the boundary.

Variational Formulation

Let $(\cdot,\cdot)_{\Omega}$ denote the standard inner product on $L^2(\Omega)$. We define the functional spaces for admissible solutions of velocity and pressure to be $\boldsymbol{\mathcal{S}}_{\mathrm{u}}$ and $\mathcal{S}_{\mathrm{p}}$, respectively. The combined space of velocity and pressure solutions is denoted by $\boldsymbol{\mathcal{S}}_{\mathrm{up}} := \boldsymbol{\mathcal{S}}_{\mathrm{u}} \times \mathcal{S}_{\mathrm{p}}$. Similarly, the test function space is $\boldsymbol{\mathcal{V}}_{\mathrm{up}} := \boldsymbol{\mathcal{V}}_{\mathrm{u}} \times \mathcal{V}_{\mathrm{p}}$.

The momentum equation (1) is multiplied by $\mathbf{v} \in \boldsymbol{\mathcal{V}}_{\mathrm{u}}$ and integrated over the domain Ω. The viscous term and the pressure term are integrated by parts; to the resulting boundary integrals, the boundary condition (4) is applied. Analogously, the continuity equation (2) is multiplied by $q \in \mathcal{V}_{\mathrm{p}}$ and integrated over Ω.

Combining both the momentum and the continuity equation in one equation yields the weighted residual formulation of the problem: find $(\mathbf{u}, p) \in \boldsymbol{\mathcal{S}}_{\mathrm{up}}$ such that for all $(\mathbf{v}, q) \in \boldsymbol{\mathcal{V}}_{\mathrm{up}}$ it holds

$$\mathcal{B}_{\mathrm{NS}}(\mathbf{v}, q; \mathbf{u}, p) = \ell(\mathbf{v}) \tag{5}$$

for $0 < t \leq T$ and $\mathbf{u}(\cdot, 0) = \mathbf{u}_0$. The form $\mathcal{B}_{\mathrm{NS}}(\mathbf{v}, q; \mathbf{u}, p)$ is defined by the terms on the left hand side, i.e.,

$$\begin{aligned}\mathcal{B}_{\mathrm{NS}}(\mathbf{v}, q; \mathbf{u}, p) &= (\mathbf{v}, \partial_t \mathbf{u})_{\Omega} + (\mathbf{v}, \nabla \cdot (\mathbf{u} \otimes \mathbf{u}))_{\Omega} \\ &+ (\varepsilon(\mathbf{v}), 2\nu\, \varepsilon(\mathbf{u}))_{\Omega} - (\nabla \cdot \mathbf{v}, p)_{\Omega} - (q, \nabla \cdot \mathbf{u})_{\Omega}\end{aligned} \tag{6}$$

whereas the linear form $\ell(\mathbf{v})$ includes forcing term and the Neumann boundary condition:

$$\ell(\mathbf{v}) = (\mathbf{v}, \mathbf{f})_{\Omega} + (\mathbf{v}, \mathbf{h})_{\Gamma_{\mathrm{N}}} \tag{7}$$

Variational Multiscale Method

The variational multiscale method was introduced in Hughes *et al.* (1998) as a general framework for computational mechanics with the objective to derive suitable mathematical models and numerical methods for multiscale phenomena. The variational multiscale method is built upon the variational form of the problem, that is, equation (5) for the Navier-Stokes equations. Starting point is a sum decomposition of the solution as

$$\mathbf{u} = \mathbf{u}^h + \hat{\mathbf{u}}, \quad p = p^h + \hat{p} \tag{8}$$

The variable $\mathbf{u}^h$ is resolved numerically, while $\hat{\mathbf{u}}$ is to be eliminated from the problem in $\mathbf{u}^h$. The impact of $\hat{\mathbf{u}}$ to the equations shall yet be conserved.

Similarly, the test functions are decomposed as

$$\mathbf{v} = \mathbf{v}^h + \hat{\mathbf{v}}, \quad q = q^h + \hat{q} \tag{9}$$

The ansatz for the admissible solutions (8) is inserted into the weak form (5). Now, it is tested separately with "resolved" test functions $(\mathbf{v}^h, q^h) \in \boldsymbol{\mathcal{V}}^h_{\mathrm{up}}$ and "unresolved" test functions $(\hat{\mathbf{v}}, \hat{q}) \in \hat{\boldsymbol{\mathcal{V}}}_{\mathrm{up}}$. The result is a system of two equations:

$$\mathcal{B}_{\mathrm{NS}}\left(\mathbf{v}^h, q^h; \mathbf{u}^h + \hat{\mathbf{u}}, p^h + \hat{p}^h\right) = \ell\left(\mathbf{v}^h\right) \tag{10}$$

$$\mathcal{B}_{\mathrm{NS}}\left(\hat{\mathbf{v}}, \hat{q}; \mathbf{u}^h + \hat{\mathbf{u}}, p^h + \hat{p}^h\right) = \ell\left(\hat{\mathbf{v}}\right) \tag{11}$$

where the first equation is to hold for all $\left(\mathbf{v}^h, q^h\right) \in \boldsymbol{\mathcal{V}}^h_{\mathrm{up}}$ and the second one for all $(\hat{\mathbf{v}}, \hat{q}) \in \hat{\boldsymbol{\mathcal{V}}}_{\mathrm{up}}$. The equation projected onto the space of unresolved scales (11) is not solved for and will be omitted. To equation (10), a linearization technique (Hughes *et al.*, 2000) is applied, yielding

$$\begin{aligned}\mathcal{B}_{\mathrm{NS}}\left(\mathbf{v}^h, q^h; \mathbf{u}^h, p^h\right) &= \ell\left(\mathbf{v}^h\right) \\ &- \mathcal{B}^1_{\mathrm{NS}}\left(\mathbf{v}^h, q^h; \mathbf{u}^h; \hat{\mathbf{u}}, \hat{p}\right) - \mathcal{B}^2_{\mathrm{NS}}\left(\mathbf{v}^h; \hat{\mathbf{u}}\right)\end{aligned} \tag{12}$$

where $\mathcal{B}^1_{\mathrm{NS}}\left(\mathbf{v}^h, q^h; \mathbf{u}^h; \hat{\mathbf{u}}, \hat{p}\right)$ contains linear terms in the unresolved quantities, while $\mathcal{B}^2_{\mathrm{NS}}\left(\mathbf{v}^h; \hat{\mathbf{u}}\right) = \left(\mathbf{v}^h, \hat{\mathbf{u}} \cdot \nabla\hat{\mathbf{u}}\right)_{\Omega}$ contains the quadratic contribution from convection, see, e.g., Gravemeier (2006b) for elaboration.

Three-Scale Separation. The separation into two different scales, resolved and unresolved quantities, can be extended to a third scale group as described, for instance, in Gravemeier (2006b). The additional group is used to further distinguish the resolved part: large resolved scales and small resolved scales. This means that a decomposition of the form

$$\mathbf{u} = \underbrace{\bar{\mathbf{u}}^h + \mathbf{u}'^h}_{\mathbf{u}^h} + \hat{\mathbf{u}}, \quad p = \underbrace{\bar{p}^h + p'^h}_{p^h} + \hat{p} \tag{13}$$

is obtained for the admissible solution functions and similarly for the test functions. As done above, this approach is inserted into the weak form (5) and tested with the individual test functions separately. The equation projected onto the space of unresolved scales is omitted, leading to a two-equation system projected onto the space of resolved scales:

$$\begin{aligned}\mathcal{B}_{\mathrm{NS}}\left(\bar{\mathbf{v}}^h, \bar{q}^h; \mathbf{u}^h, p^h\right) &= \ell\left(\bar{\mathbf{v}}^h\right) \\ &- \mathcal{B}^1_{\mathrm{NS}}\left(\bar{\mathbf{v}}^h, \bar{q}^h; \mathbf{u}^h; \hat{\mathbf{u}}, \hat{p}\right) - \mathcal{B}^2_{\mathrm{NS}}\left(\bar{\mathbf{v}}^h; \hat{\mathbf{u}}\right)\end{aligned} \tag{14}$$

$$\begin{aligned}\mathcal{B}_{\mathrm{NS}}\left(\mathbf{v}'^h, q'^h; \mathbf{u}^h, p^h\right) &= \ell\left(\mathbf{v}'^h\right) \\ &- \mathcal{B}^1_{\mathrm{NS}}\left(\mathbf{v}'^h, q'^h; \mathbf{u}^h; \hat{\mathbf{u}}, \hat{p}\right) - \mathcal{B}^2_{\mathrm{NS}}\left(\mathbf{v}'^h; \hat{\mathbf{u}}\right)\end{aligned} \tag{15}$$

It can be seen from this system that the equation in the large resolved scales (14) is accessible independently from the equation in the small resolved scales (15).

Variational Multiscale Large Eddy Simulation

The system (14)-(15) still contains the unresolved variables $\hat{\mathbf{u}}$ and $\hat{p}$. The next step towards an implementation of the method is to determine which effect the terms $\mathcal{B}^1_{\mathrm{NS}}$ and $\mathcal{B}^2_{\mathrm{NS}}$ actually have within the Navier-Stokes equations. An established approach for representing the effect of the unresolved scales is LES with a Smagorinsky model. It aims to reintroduce the insufficiently resolved dissipation in the form of an additional viscous term, i.e., by approximating the terms $\mathcal{B}^{1/2}_{\mathrm{NS}}$ on the right hand side of (12) by an additional viscous term, the so-called *subgrid viscosity*, cf. Sagaut (2006).

The derivation of a traditional LES in this form was the basis for a further development of the method, leading to a *variational multiscale Large Eddy Simulation* (VMLES). The method is applied to the three-scale separation derived in (14)-(15). Turbulence theory specifies that energy transport occurs mainly between neighboring scale groups. This observation motivates the restricted application of a subgrid-viscosity model only to the small resolved scales, which are closer to the unresolved scales in the scale spectrum. Large resolved scales, on the other hand, will not be influenced directly by any model. Hence, the approximations

$$\mathcal{B}^1_{\mathrm{NS}}\left(\bar{\mathbf{v}}^h, \bar{q}^h; \mathbf{u}^h; \hat{\mathbf{u}}, \hat{p}\right) + \mathcal{B}^2_{\mathrm{NS}}\left(\bar{\mathbf{v}}^h; \hat{\mathbf{u}}\right) \approx 0 \tag{16}$$

$$\mathcal{B}^1_{\mathrm{NS}}\left(\mathbf{v}'^h, q'^h; \mathbf{u}^h; \hat{\mathbf{u}}, \hat{p}\right) + \mathcal{B}^2_{\mathrm{NS}}\left(\mathbf{v}'^h; \hat{\mathbf{u}}\right) \approx \left(\varepsilon(\mathbf{v}'^h), 2\nu'_T \varepsilon(\mathbf{u}'^h)\right)_\Omega \tag{17}$$

are used. To the small resolved scales, an adopted subgrid-viscosity model is applied. The small-scale subgrid viscosity is defined by a slightly modified Smagorinsky model as

$$\nu'_T = (C_{\mathrm{S}} h)^2 \left|\varepsilon(\mathbf{u}'^h)\right| \tag{18}$$

with C_{S} denoting the Smagorinsky constant, h the element size and $\left|\varepsilon(\mathbf{u}'^h)\right| = \sqrt{2\varepsilon(\mathbf{u}'^h) : \varepsilon(\mathbf{u}'^h)}$ the norm of the small-scale velocity gradient.

Inserting the approximations (16) into (14) and (17) into (15) yields the final system

$$\mathcal{B}_{\mathrm{NS}}\left(\mathbf{v}^h, q^h; \mathbf{u}^h, p^h\right) + \left(\varepsilon(\mathbf{v}'^h), 2\nu'_T \varepsilon(\mathbf{u}'^h)\right)_\Omega = \ell\left(\mathbf{v}^h\right) \tag{19}$$

which is to hold for all test functions $\left(\mathbf{v}^h, q^h\right) \in \boldsymbol{\mathcal{V}}^h_{\mathrm{up}}$.

VMLES IMPLEMENTATION BASED ON FEM

For an implementation of the VMLES (19), the small-scale variables $\mathbf{u}'^h$ and $\mathbf{v}'^h$ have to be correctly defined. Within the framework of a finite element method (FEM), there are two possible ways to separate small from large resolved scales (Gravemeier, 2006b):

p-type Scale Separation One possibility to distinguish between different scale groups within a FEM is to assign different polynomial orders to basis functions of large resolved scales and small resolved scales, respectively. Lower-order basis functions constitute large resolved scales, and higher-order functions constitute small resolved scales. This can be done either by using hierarchical basis functions, where the basis functions are ordered by their polynomial order, or an L^2-projection onto a lower-order subspace.

h-type Scale Separation The second class of scale-separating approaches makes use of different grids. A coarse grid constitutes the large-scale variables $\bar{\mathbf{u}}^h$ and $\bar{p}^h$, whereas a finer grid specifies the variables at the full resolution level $\mathbf{u}^h$ and p^h. The developments in the following are based on an h-type scale separation within a nodal-based FEM with (tri-) linear basis functions.

h-type Scale Separation

An h-type scale separation requires the introduction of a second grid. It is assumed that a coarse grid is given, constituted of so-called *parent elements*. Each parent element is isotropically subdivided into a predefined number of *child elements*. The union of all child elements represents the actual resolution limit of the discretization and hence defines the variables

$$\mathbf{u}^h(\mathbf{x}, t) = \sum_{A=1}^{n_{\mathrm{u,tot}}} \varphi_A(\mathbf{x})\, \mathbf{u}_A(t) \tag{20}$$

$$p^h(\mathbf{x}, t) = \sum_{A=1}^{n_{\mathrm{p,dof}}} \psi_A(\mathbf{x})\, p_A(t) \tag{21}$$

Figure 1: 1D illustration of the basis functions φ on the full resolution level and the large-scale basis functions $\bar{\varphi}$.

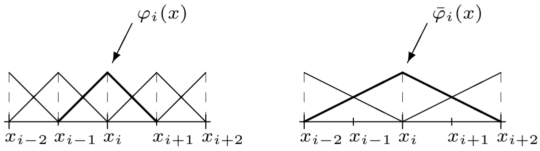

Figure 2: 1D illustration of the construction of the small-scale part $\mathbf{u}'^h$ from $\mathbf{u}^h$ and the large-scale part $\bar{\mathbf{u}}^h$.

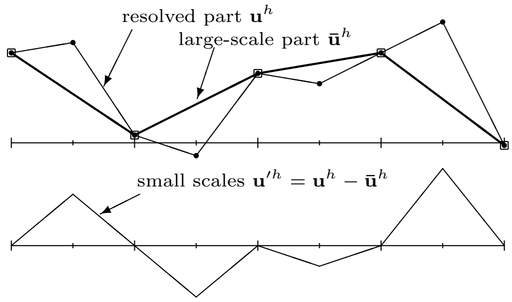

Note that some of the velocity degrees of freedom may be fixed by Dirichlet boundary conditions.

The evaluation of the subgrid viscosity term in (19) involves small resolved quantities. These are, however, not directly available, since the fine grid also contains coarse-scale proportions. Hence, we define the small resolved velocity indirectly as

$$\mathbf{u}'^h(\mathbf{x}, t) = \mathbf{u}^h(\mathbf{x}, t) - \bar{\mathbf{u}}^h(\mathbf{x}, t) \tag{22}$$

where we use the definition of $\mathbf{u}^h$ in equation (13). In analogy to (20), the large-scale velocity is given in the usual FE manner by a weighted sum of basis functions, i.e.,

$$\bar{\mathbf{u}}^h(\mathbf{x}, t) = \sum_{\bar{A}=1}^{\bar{n}_{\mathrm{u,tot}}} \bar{\varphi}_{\bar{A}}(\mathbf{x})\, \bar{\mathbf{u}}_{\bar{A}}(t) \tag{23}$$

The coefficients $\bar{\mathbf{u}}_{\bar{A}}(t)$ correspond to the coarse-scale approximation of the velocity at the nodes of the parent elements. The basis functions $\bar{\varphi}_{\bar{A}}$ are nodal-based piecewise linear functions similar to the ones at the child level, but their support is twice as large, see figure 1.

Figure 2 indicates that for linear elements, the nodes from parent elements are also available on the child grid. This means that the coefficients $\bar{\mathbf{u}}_{\bar{A}}(t)$ can be directly compared with the coefficients $\mathbf{u}_A(t)$ for indices A that are related to nodal points at the parent level.
Hence, the small-scale part $\mathbf{u}'^h$ can be expressed in terms of the coefficients $\mathbf{u}_A(t)$ and the basis functions φ_A and $\bar{\varphi}_A$ as

$$\mathbf{u}'^h(\mathbf{x}, t) = \sum_{A \in \bar{\eta} \cap \eta} \left(\varphi_A(\mathbf{x}) - \bar{\varphi}_A(\mathbf{x})\right) \mathbf{u}_A(t) + \sum_{A \in (\eta \setminus \bar{\eta})} \varphi_A(\mathbf{x})\, \mathbf{u}_A(t) \tag{24}$$

where $\eta = \{1, \ldots, n_{\mathrm{u,dof}}\}$ is the set of nodal points at the full resolution level and $\eta = \{1, \ldots, \bar{n}_{\mathrm{u,dof}}\} \subset \eta$ the subset of parent nodal points.

Expression (24) as well as a similar expression for the small-scale test function $\mathbf{v}'^h$ are used to perform the element integrations. Thus, the additional term is now compatible to standard FEM algorithms.

NUMERICAL RESULTS FOR TURBULENT FLOW IN A DIFFUSER

The diffuser geometry is shown in figure 3. In the inflow channel, the inflow velocity $\mathbf{u}^{\text{in}}(t)$ for the actual diffuser is generated. No-slip boundary conditions are assumed at the upper and lower walls Γ_{w}. A convective boundary condition is prescribed at the outflow boundary Γ_{out}, and periodic boundary conditions are assumed on the boundaries Γ_{per} in x_3-direction. The diffuser, including inlet and outlet channel, is discretized using 290, 64, and 80 control volumes in x_1-, x_2-, and x_3-direction, respectively.

To perform calculations, an h-type VMLES within a finite volume method (FVM) was developed. The method was implemented into the CDP-α code, the flagship LES code of the Center for Turbulence Research at Stanford University. The control volumes are uniformly distributed in the spanwise direction. In the wall-normal direction, a cosine function for refinement towards the walls for the parent grid is used, with the isotropic hierarchical subdivision procedure subsequently applied. In the streamwise direction, the following control volume distribution is employed: in the inlet channel, h_1 decreases linearly from 0.15 to 0.05, in the asymmetric diffuser section, h_1 increases linearly from 0.05 to 0.475, in the first section of the outlet channel (up to $x_1 = 74.5$), h_1 increases linearly from 0.475 to 0.825, and in the remaining section of the outlet channel, the control volumes are uniformly distributed with $h_1 = 0.825$. Comparing the discretization of the diffuser to the finer discretization in the Wu-LES (Wu *et al.*, 2004), which employed 590, 100, and 110 control volumes in x_1-, x_2-, and x_3-direction, it is stated that less than 23% the number of control volumes are used in the present case.

Three different methods are investigated: the dynamic Smagorinsky (DS) model in a non-multiscale application (see Germano *et al.*, 1991), the constant-coefficient-based Smagorinsky model within the multiscale environment (CMS), and the dynamic Smagorinsky model within the multiscale environment (DMS). All of these methods are analyzed for a projective scale-separating operator S^{pm} as defined in Gravemeier (2006a). The abbreviation "DMS-PM", for instance, indicates the variational multiscale LES incorporating a dynamic Smagorinsky model, with the scale-separating operator S^{pm} applied. In addition, a non-projective scale-separating operator S^{sm} (smoothing prolongation) is investigated for CMS, since this method revealed the most notable differences between the scale-separating operators for the test case in Gravemeier (2006a). Results are also reported for simulations using no model at all (NM), which represents a coarse (i.e., not sufficiently resolved) DNS. The Wu-LES, which the results are compared to, applied the same dynamic Smagorinsky model in a traditional non-multiscale LES (i.e., DS using smooth filters for scale separation). Evaluating the necessary computational effort provides the following numbers. Setting the computational effort for NM to 1.0, the relative measures for CMS-PM, CMS-SM, DS-PM and DMS-PM are approximately 1.08, 1.34, 1.27, and 1.32, respectively. These numbers are even more impressively in favor of CMS-PM than the ones for the channel in Gravemeier (2006a). Thus, it is confirmed that CMS in combination with PM is a very efficient method computationally, in the present case substantially more efficient than, for instance, DS. Using the scale-separating operator SM, the numbers increase drastically for CMS. Less effort is required for PM compared to SM for reasons explained in Gravemeier (2006a).

Figure 3: Diffuser geometry in x_1-x_2-plane

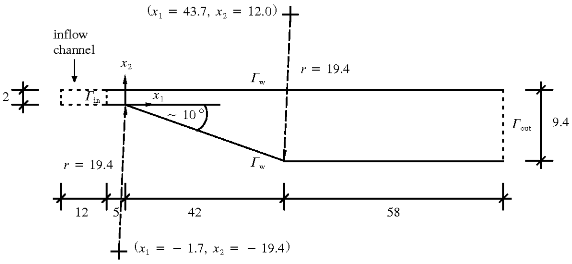

Figure 4: Skin friction coefficient (factor 1000) along the upper wall of the diffuser

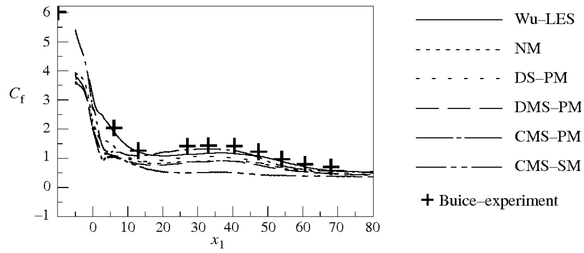

As one sample of the flow parameters investigated, figure 4 depicts the results for the skin friction coefficient along the upper wall of the diffuser. Results for further flow parameters can be found in Gravemeier (2007). It is stated that all methods tend to underpredict C_f compared to the results from the Wu-LES and the Buice-experiment (Buice and Eaton, 1997). The worst results are produced by CMS-SM. The profile for NM is closest to the ones from the Wu-LES and the Buice-experiment immediately behind the diffuser throat, but gets worse in its prediction further downstream. DS-PM yields a fairly good prediction throughout the diffuser, and DMS-PM produces worse results than DS-PM. Although the results for CMS-PM are worse than the ones for NM immediately behind the diffuser throat, the prediction is the best overall. It is the only method yielding results which almost match the experimental results in the section of the diffuser between $x_1 \approx 18$ and $x_1 \approx 46$. In this part of the diffuser, which is approximately the region where the flow is separated, CMS-PM appears to produce even better results than the substantially finer discretized Wu-LES. Furthermore, it seems to be the only one of the present methods which would have been able to predict the first point from the Buice-experiment at $x_1 \approx -10$, if the inlet channel had been elongated.

1D FOURIER ANALYSIS OF VMLES

In order to understand the impact of the subgrid-viscosity model applied to the small resolved scales, Kronbichler (2007) analyzed it with tools from Fourier analysis. To this end, it is assumed that the subgrid viscosity ν_T' is constant, namely $\nu_T' = 1$ in (19). Additionally, the analysis is performed using an equation with only one space dimension in the unit interval $\Omega = (0, 1)$. The domain Ω is divided into $\bar{n}$ equal-sized parent elements. Each parent element is isotropically divided into two child elements, such that the full discretization consists of $n = 2\bar{n}$ elements of size $h = 1/n$. The basis functions φ_A and $\bar{\varphi}_A$ are depicted in figure 1.

Except the subgrid viscosity term and the time derivative of $\mathbf{u}$, all terms in the Navier-Stokes equations (1)-(2) are omitted. The result is a parabolic-like equation, which is completed by homogeneous Dirichlet boundary conditions.

Since the subgrid viscosity $\big(\varepsilon(\mathbf{v}'^h), 2\nu'_T\varepsilon(\mathbf{u}'^h)\big)_\Omega$ is purely diffusive, it is reasonable to compare it to a standard viscous term $\big(\varepsilon(\mathbf{v}^h), 2\nu_T\varepsilon(\mathbf{u}^h)\big)_\Omega$, as it is also introduced by a standard Smagorinsky model. In one spatial dimension, this means that the discretized parabolic-like equation including the subgrid-viscosity term is compared to the usual heat equation, i.e.,

$$\Big(v^h, \partial_t u^h\Big)_\Omega = -\Big(\partial_x v'^h, \partial_x u'^h\Big)_\Omega \tag{25}$$

$$\Big(v^h, \partial_t u^h\Big)_\Omega = -\Big(\partial_x v^h, \partial_x u^h\Big)_\Omega \tag{26}$$

Here, the variables u^h and v^h denote the usual finite element approximations of the solution and the respective test functions, and u'^h and v'^h the small-scale quantities.

Semi-Discretization in Space – System of ODE

As done above for the general equations, (20) and (24) are inserted into the equations (25) and (26), respectively. Performing the element integration and subsuming the coefficients u_A to one vector $\mathbf{u}$ leads to a system of ordinary differential equations in time.

For the *parabolic-like equation including the subgrid-viscosity term*, we obtain the system

$$\mathbf{M}_h \partial_t \mathbf{u} = \mathbf{K}_h^{\mathrm{sv}} \mathbf{u} \tag{27}$$

where the $(n-1)\times(n-1)$ mass matrix[1] is given by

$$\mathbf{M}_h = \frac{h}{4}\begin{pmatrix} 2 & 1 & & & \\ 1 & 2 & 1 & & \\ & \ddots & \ddots & \ddots & \\ & & 1 & 2 & 1 \\ & & & 1 & 2 \end{pmatrix} \tag{28}$$

and the $(n-1)\times(n-1)$ stiffness matrix by

$$\mathbf{K}_h^{\mathrm{sv}} = \frac{1}{2h}\begin{pmatrix} -4 & 2 & & & & & & \\ 2 & -2 & 2 & -1 & & & & \\ & 2 & -4 & 2 & & & & \\ & -1 & 2 & -2 & 2 & -1 & & \\ & & \ddots & \ddots & \ddots & \ddots & \ddots & \\ & & & & 2 & -4 & 2 & \\ & & & & -1 & 2 & -2 & 2 \\ & & & & & & 2 & -4 \end{pmatrix} \tag{29}$$

Similarly, the *standard heat equation* results in

$$\mathbf{M}_h \partial_t \mathbf{u} = \mathbf{K}_h^{\mathrm{heat}} \mathbf{u} \tag{30}$$

with the mass matrix (28) as above and the stiffness matrix

$$\mathbf{K}_h^{\mathrm{heat}} = \frac{1}{h}\begin{pmatrix} -2 & 1 & & & \\ 1 & -2 & 1 & & \\ & \ddots & \ddots & \ddots & \\ & & 1 & -2 & 1 \\ & & & 1 & -2 \end{pmatrix} \tag{31}$$

Obviously, the stiffness matrices $\mathbf{K}_h^{\mathrm{sv}}$ and $\mathbf{K}_h^{\mathrm{heat}}$ mainly drive the solution to the individual equations (25) and (26). To learn about the properties, the eigenvalues and corresponding eigenvectors of the matrices are calculated. This can be done analytically for the heat equation via a Fourier analysis.

[1]Due to the Dirichlet b.c., only $n-1$ inner points are left.

Figure 5: Eigenvalues against wave number of eigenvectors for stiffness matrix $\mathbf{K}_h^{\mathrm{heat}}$, total system in (30) and exact differential operator ∂_{xx} at $n = 40$.

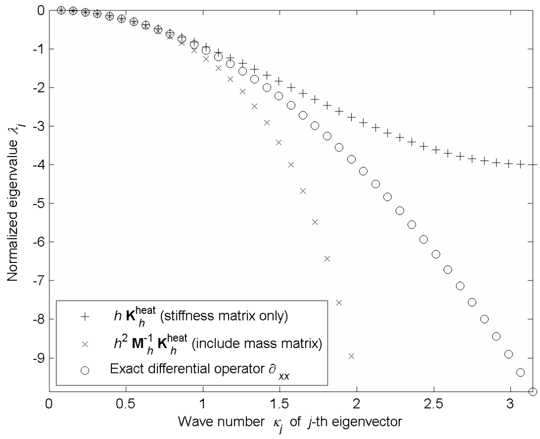

Fourier Analysis for the Heat Equation

The special structure of the matrix $\mathbf{K}_h^{\mathrm{heat}}$ gives rise to a homogeneous difference equation. When trying to find an eigenvalue, the equation $\mathbf{K}_h^{\mathrm{heat}}\mathbf{y} = \lambda\mathbf{y}$ for some eigenvector $\mathbf{y} \neq \mathbf{0}$ is to be solved. This is equivalent to solving the homogeneous difference equation

$$\frac{1}{h}\left(u_{k-1} - (2 + h\lambda)u_k + u_{k+1}\right) = 0 \tag{32}$$

with homogeneous boundary data $u_0 = u_n = 0$. The Fourier ansatz is a plane wave $u_k = \mathrm{e}^{\mathrm{i}\pi x_k j}$ with $x_k = k/n$ denoting the spatial position and $j = 1,\dots,n$ the wave parameter. Using the boundary conditions gives the eigenvector $\mathbf{y}^{(j)} = (u_1^{(j)},\dots,u_{n-1}^{(j)})^T$ as

$$u_k^{(j)} = \sin\left(\frac{jk\pi}{n}\right) \tag{33}$$

for the j-th eigenvalue

$$\lambda_j = -\frac{2}{h}\left(1 - \cos\left(\frac{j\pi}{n}\right)\right) = -\frac{4}{h}\sin^2\left(\frac{j\pi}{2n}\right) \tag{34}$$

Hence, the eigenvector $\mathbf{y}^{(j)}$ to the eigenvalue λ_j is a plane wave with normalized wave number $\kappa_j = j\pi/n$. This makes it possible to display the eigenvalues related to the relevant parameter of the eigenvector, namely the wave number κ_j. Figure 5 displays the run of the eigenvalue λ_j of the (normalized) matrix $h\mathbf{K}_h^{\mathrm{heat}}$ with the wave number κ_j. The figure includes the run of the eigenvalues for the full matrix in (30), i.e., after including the mass matrix. The eigenvalues of $h^2\mathbf{M}_h^{-1}\mathbf{K}_h^{\mathrm{heat}}$ differ from (34) by the term $1/2(1+\cos(j\pi/n))$ in the denominator. Figure 5 is completed by the properties of the exact differential operator ∂_{xx} (spectral differentiation), where the normalized eigenvector to κ_j is $-\kappa_j^2$.

Application of Fourier Techniques to Subgrid Viscosity

The Fourier technique introduced above can be used to get an estimate for the eigenvalues of the more complicated stiffness matrix $\mathbf{K}_h^{\mathrm{sv}}$. As can be seen, the rows of the matrix are in turn given by a three-term recursion and a five-term recursion, respectively. The five-term recursion stems from

Figure 6: Eigenvalues against wave number of eigenvectors for VMLES stiffness matrix $\mathbf{K}_h^{\mathrm{sv}}$, eigenvalue estimate with Fourier theory at $n = 40$. Note the difference between VMLES and standard LES (i.e., using $\mathbf{K}_h^{\mathrm{heat}}$) at low wave number κ_j.

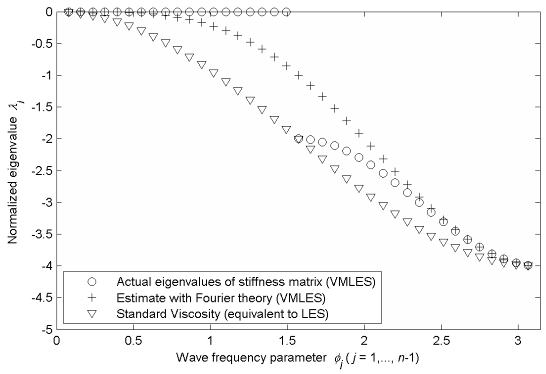

even grid points with parent-element basis functions present, whereas the three-term recursion is obtained at odd child-only points, cf. figure 1 for the grid construction. Hence, an approximation of the eigenvalues is obtained by calculating the solutions to each of these recursions (with eigenvalues $\lambda_j^{(\mathrm{e})}$ and $\lambda_j^{(\mathrm{o})}$, respectively) and build the final eigenvalue by an average of both solutions:

$$\begin{aligned}\lambda_j^{\mathrm{sv,est}} &= \frac{1}{2}\left(\lambda_j^{(\mathrm{e})} + \lambda_j^{(\mathrm{o})}\right) \\ &= \frac{1}{2h}\left(-3 + 4\cos(\phi_j) - \cos(2\phi_j)\right).\end{aligned} \tag{35}$$

In addition to this eigenvalue estimate, the true eigenvalues and eigenvectors of the matrix are calculated numerically at $n = 40$. Figure 6 compares the true eigenvalues with the estimate (35). The exact eigenvectors are no longer plane waves, though. Nonetheless, they are quite close to plane waves, making the comparison in terms of wave numbers in figure 6 a good qualitative description.

Figure 6 includes a comparison between the small-scale subgrid viscosity from the VMLES to the subgrid viscosity of a traditional LES. It can be seen from the figure that there is indeed no viscosity at the larger resolved scales for the VMLES, while there is a notable viscosity for the traditional LES. This supports that the above construction with two grids does indeed impose the subgrid viscosity only to small scales.

Fourier Analysis: Tool to compare Scale-Separating Methods

The eigenvalue analysis with Fourier techniques has been used to characterize the properties of the small-scale subgrid viscosity introduced by the VMLES. This characterization can be applied to other scale-separating approaches as for example the one used in Gravemeier (2006a, 2007). The different performance of the individual scale-separating operators may already be explained by their eigenvalues for a one-dimensional test equation like (25). For instance, other scale-separating operators may lead to a eigenvalue distribution similar to the estimated eigenvalue distribution according to (35), that is, the transition from non-influenced to influenced scales may be gradual and not sharp as it actually is for the h-type separation used above. Similarly, the Fourier analysis can help in comparing the used h-type scale separation to a p-type scale separation as well as identifying possible differences and similarities.

CONCLUSIONS

The framework of the variational multiscale method has been used to derive a method for variational multiscale large eddy simulation of turbulent flows. The influence of the subgrid-viscosity model is restricted to the smaller of the resolved scales, whereas the large resolved scales are left without the addition of a modeling term. The separation between large and small resolved scales has been demonstrated for a finite element method using multiple grids, one to define large resolved scales and the finer one for the whole resolution limit. However, this approach is also applicable to a finite volume method. The results for a simulation of a turbulent diffuser flow have shown the good performance of the VMLES for relatively coarse grids and indicated its great potential for high-fidelity simulations of turbulent flows.

A Fourier analysis of a linearized subgrid-viscosity term has been introduced as a tool to analyze scale-separating methods. With this approach, various scale-separating procedures can be compared, without implementing them fully in a three-dimensional code. This may give first indications concerning similarities and differences of the individual approaches.

REFERENCES

Buice, C.U., Eaton, J.K., 1997, "Experimental investigation of flow through an asymmetric plane diffuser". TSD-107, Department of Mechanical Engineering, Stanford University.

Germano, M., Piomelli, U., Moin, P., and Cabot, W. H., 1991, "A dynamic subgrid-scale eddy vicosity model", *Phys. Fluids*, Vol. 3, pp. 1760-1765.

Gravemeier, V., 2006a, "Scale-separating operators for variational multiscale large eddy simulation of turbulent flows", *J. Comput. Phys.*, Vol. 212, pp. 400-435.

Gravemeier, V., 2006b, "The variational multiscale method for laminar and turbulent flow", *Arch. Comput. Meth. Engng.*, Vol. 13, 2, pp. 249-324.

Gravemeier, V., 2007, "Variational multiscale large eddy simulation of turbulent flow in a diffuser", *Comput. Mech.*, Vol. 39, 4, pp. 477-495

Hughes, T.J.R., Feijó, G.R., Mazzei, L., and Quincy, J., 1998, "The variational multiscale method – a paradigm for computational mechanics", *Comput. Meth. Appl. Mech. Engrg.*, Vol. 166, pp. 3-24.

Hughes, T.J.R., Mazzei, L., and Jansen, K.E., 2000, "Large eddy simulation and the variational multiscale method", *Comput. Visual. Sci.*, Vol. 3, pp. 47-59.

Kronbichler, M., 2007, "Finite-element based variational multiscale methods for large eddy simulation of turbulent flows", Diploma Thesis, Zentrum Mathematik, Technische Universität München, Germany.

Sagaut, P., 2006, "Large eddy simulation for incompressible flows", 3rd edition, Springer-Verlag, Berlin.

Wu, X., Schlueter, J., Moin, P., Pitsch, H., Iaccarino, G., Ham, F., 2006, "Computational study on the internal layer in a diffuser", *J. Fluid Mech.*, Vol. 550, pp. 391-412.